A Numerical Simulation on the Airfoil S833 Equipped with Flapping Trailing Edge Fringes

H. Yu and Z. Yang[†]

Department of Mechanical and Material Engineering, Wright State University, Dayton, OH, 45435, USA

†*Corresponding Author Email: zifeng.yang@wright.edu*

ABSTRACT

Design optimization has been increasingly investigated for an airfoil, aiming to reduce the vorticity in the wake and increase the aerodynamic performance. In the current work, a two-dimensional (2D) S833 airfoil equipped with a flapping fringe at the trailing edge has been studied using computational fluid dynamics (CFD) simulations. The objective is to investigate the influence of the length (L_f) and flapping frequency (f) of the fringe on shedding vortices from the airfoil and the drag and lift coefficients. The validation of the current numerical approach for both static and dynamic motions of the airfoil was conducted. First, four different computational meshes were created for the static bare airfoil S833 model, and the simulated drag and lift coefficients were compared against experimental results. It is observed that the second finest mesh contributes to the best agreement with the measurement data. In addition, the numerical accuracy of the dynamic simulation was assessed by reproducing the pressure distribution around the airfoil NACA0014 with a periodic plunging motion at different time phases within one plunging cycle. Good agreements between the simulated and previous computational results are obtained. Moreover, the investigation of S833 airfoil equipped with a flapping fringe reveals that the model with L_f =0.01 m (10% of the chord length) associated with a flapping frequency below the shedding frequency of the bare airfoil can significantly alter the coherent structure of the shedding vortices, breaking the routine large-scale vortex into small-scale weak vortices. It also results in reducing the intensity of vortices and shortening the distance between each pair of vortices to accelerate the dissipation of vorticity. In addition, the equipped flapping trailing edge fringe can achieve extra benefit in aerodynamic performance in terms of the reduction of the drag coefficients and the enhancement of lift coefficients.

Keywords: S833 Airfoil; Flapping fringe; Vortex shedding; Flapping frequency.

NOMENCLATURE

A	amplitude of the flapping angle of the trailing edge fringe	p_∞	free stream air pressure
c	chord length	R_e	Reynolds number based on airfoil chord length
C_L	lift coefficient of the airfoil	S_t	Strouhal number defined as $St = fd/U_\infty$
C_D	drag coefficient of the airfoil	T	time
C_P	pressure coefficient defined as $C_p = (p - p_\infty)/(0.5\rho U_\infty^2)$	T	time period of the flapping motion of the trailing edge fringe
f	frequency of shedding vortex	U_∞	free stream velocity
h	instantaneous position of the airfoil for the plunge motion		
h_o	dimensionless stroke amplitude	f_s	frequency of shedding vortex for bare airfoil model
L_f	length of the flapping fringe	Θ	deflection angle of the trailing edge fringe
P	air pressure in the flow field	Ω	angular frequency of the plunging motion
P	density of airflow		

1. INTRODUCTION

The silent flight of owls has drawn interests from researchers for decades. It has been found that the comb-like leading edge serves as vortex generators, which results in streamwise vortices over the wing to suppress the laminar separation from the leading edge at a high angle of attack. On the other hand,

the main noise source from the trailing edge of the wing is eliminated by the soft trailing edge fringe through the alteration of the scattering mechanism. Consequently, noise above 2 kHz was effectively eliminated by the compliant surface constructed by the down feathers through a bypass dissipation mechanism (Lilley *et al.,* 1998; Sarradj *et al.,* 2011). Inspired by the owl's wing, the serrated leading edge, compliant surface, and flexible trailing edge fringe have been investigated to improve the aerodynamic performance and reduce the noise of airfoils (Moreau *et al.,* 2013; Winzen *et al.,* 2014; and Winzen *et al.,* 2012). Klan *et al.* (2009) and Winzen *et al.* (2014) conducted experimental investigations to compare the flow around the natural and modeled owl wing and found that the compliant surface of the natural wing could maintain an attached flow effectively while the rigid owl wing model showed separation at the same angle of attack. Using owl wing inspired configuration as a passive control strategy for an airfoil model to reduce the drag and enhance the lift coefficients has gained considerable attention in the past decade (Kerho *et al.,* 1993; Klän *et al.,* 2009; Miao *et al.,* 2006; Shan *et al.,* 2008 and Veldhuis *et al.,* 2012).

Leading-edge serration has been intensively investigated, indicating that the serration serves as a vortex generator, which results in a longitudinal vortex and thus accomplishes the boundary control (Hersh *et al.,* 1974; Ito *et al.,* 2009; Klän *et al.,* 2010 & Soderman, 1973). The reduction of noise was observed with leading-edge configurations and Reynolds numbers (Hersh *et al.,* 1974, 1973 & Arndt *et al.,* 1972). The shape of the leading-edge serration can alter the noise diversely. Narayanan *et al.* (2015) implemented an experimental study to investigate the effects of the wavy leading edge on the noise reduction using a produced turbulent mean flow flowing over a flat-plate airfoil. The results indicated that with increasing the amplitude of the wavy leading edge, the sound pressure level is decreased linearly, mainly resulting from the sweep-angle effect in the hill region of the serration structure. Kim *et al.* (2016) also observed the ability of the leading-edge serration to reduce the airfoil noise because of the interference of sound radiated along the edges. In addition, the serrated trailing edge has also been studied for its impact on the aerodynamic performance, wake development and noise emission from the airfoils (Moreau *et al.,* 2013; Chong & Joeseph, 2013; Liang *et al.,* 2010; Chong *et al.,* 2013; Jones *et al.,* 2012 & Liu *et al.,* 2017). It has been confirmed that the trailing-edge serration is able to diminish the airfoil tonal noise especially when the serration angle and tip-to-root distance are large (Chong *et al.,* 2013). Moreau *et al.* (2013) showed that the trailing-edge serrations can decrease up to 13 dB in the narrowband noise levels because of the attenuation of vortex shedding at the trailing edge.

The brush-like trailing edge, which contains both a porous feature and flexibility as the natural fringe, has been adopted as the trailing edge extension to suppress both the narrowband bluntness noise and broadband turbulent boundary-layer trailing-edge noise (Finez *et al.,* 2010; Herr *et al.,* 2005; Das *et al.,* 2015 & Schlanderer *et al.,* 2015). It has been observed that more than 10 dB of the source noise reduction can be achieved by using the brush-like configuration at the trailing edge (Herr *et al.,* 2005). Kamps *et al.* (2017) conducted an experimental investigation on flow over an airfoil with a flexible trailing edge attached on the suction side of the airfoil considered as a passive control of the vortex shedding and observed a noticeable noise reduction. Furthermore, Talboys *et al.* (2019) indicated that the tonal noise can be removed when the passive flaplets are affixed to the pressure side of the airfoil, whereas the tonal noise can be attenuated if the flaplets are placed on the suction side of the airfoil. Talboys *et al.* (2018) also analyzed different motions of the trailing edge flaplet and found that the movement of the trailing edge is primarily due to small scale turbulent structures, and therefore, the flaplets are able to stabilize the shear layer on the suction side to promote the performance of the airfoil. Our experimental investigation showed that the real fringe feather edges installed on an airfoil enables the large-scale vortex to break down into small-scale turbulence (Yang *et al.,* 2015), demonstrating that the vibrating long flexible fringe contributes an important vertical velocity in the flow field around the trailing edge. As a result, it suppresses the leading-edge vortices approaching the surface of the flexible tail and accelerates the dissipation of the leading-edge vortices.

Even though numerous studies have been conducted to understand the owl's wing and utilize its feature for airfoil design, the underlying physical mechanism for noise reduction due to the flapping trailing edge fringe is still not clear. Very few studies focused on the effect of the flapping trailing edge fringe on the shedding vortices in the downstream wake, which is highly associated with the noise production and the aerodynamic performance of the airfoil. Thus, the investigation of this work primarily focuses on the sensitivity of the fringe lengths (L_f) and flapping frequencies (f) on altering the flow characteristics of the static airfoil S833. Section 2 introduces the airfoil geometry and simulation approach. The validation of both the static and dynamic motions of the airfoil is described in section 3. Finally, the characteristics of the vortex shedding in the wake and the aerodynamic performance under various fringe lengths and flapping frequencies are presented and discussed in the following sections.

2. METHODOLOGY

2.1 Setup of the Computational Model

The airfoil S833 was used to study the vortex shedding in the wake with a rigid flapping fringe equipped at the trailing edge. The detailed description of the 2D geometry and boundary conditions is shown in Fig. 1. The dimension of the outside domain is 20C (length) times 10C (width) with 5C between the inlet and the leading edge of
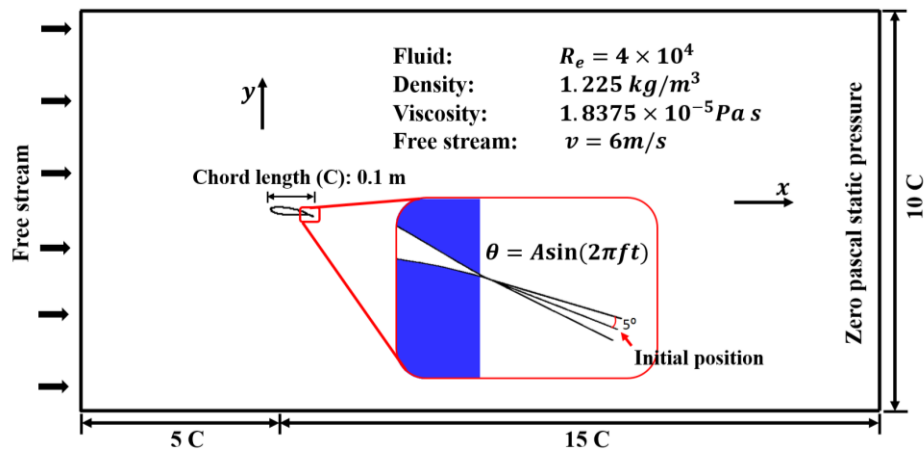
Fig. 1. Boundary conditions of the simulation of flow over the airfoil S833 equipped with a flapping trailing edge fringe.

the airfoil, where C is the chord length (0.1 m). The numerical simulation setup was defined based on the previous experimental work (Yang *et al.,* 2015), aiming to explore whether the current approach can capture the characteristics of the vortex shedding observed in the experiment. The inlet velocity was set at 6 m/s, and the density and viscosity of the air were assumed as 1.225 kg/m^3 and 1.8375×10^{-5} Pa s to obtain the Reynolds number (R$_e$) of 4×10^4 used in the experiment. The outlet boundary condition was defined as static pressure (Pressure = 0 Pa), and the airfoil and top and bottom surfaces were defined as non-slip wall condition. The angle of attack (AoA) of the airfoil is set at 9-degree. It is worth noting that the current CFD simulation results are not comparable to the experimental data since the flapping motion of the fringe in the experiment was depended upon its material (performed with a random flapping frequency). The L_f of the flapping fringe ranges from 8% to 12% of the chord length with a 2% increment, and the f ranges from 80 Hz to 170 Hz with a 30 Hz increment. The initial f was determined according to the vortex shedding frequency (f_s) from the bare airfoil model. The f_s of the bare airfoil model was 140 Hz obtained via the power spectral density (PSD) of the velocity in the wake of the airfoil, which is consistent with the experimental result (Yang *et al.,* 2015). The dynamic motion of the trailing edge fringe can be expressed by $\theta=Asin(2\pi ft)$, where θ is the deflection angle of the fringe in degree, A is the amplitude of the flapping angle and set as 5-degree (according to the observation in the experiment). The pivot point of the flapping motion is fixed at the tip of the trailing edge. The simulations were performed on a computational Cluster, which is 3.4GHz AMD Phenom II X4 965 Quad-core and 8 GB RAM, and each case was run with 32 processors. In the current study, a total simulation time of 1.5 s of the flow was performed with a time step of 5e-5 s. The mean computational time for each flapping fringe airfoil simulation is 23 hours.

2.2 Computational Fluid Dynamics Simulations

The commercial CFD software Cradle SC/Tetra

V12 (Dayton, Ohio) was used to conduct the numerical simulations. The computational solver employs the finite volume method to compute the governing continuity and momentum equations using hybrid grids, where hexahedral grids were generated around the airfoil as prism layers to capture the velocity boundary layer, and tetrahedral grids were distributed on the rest region generated by local mesh refinement technique, as shown in Fig. 2. The tetrahedral mesh was selected since it supports the adaptive mesh refinement technique by the software. The validation studies also indicated that this meshing strategy satisfies the numerical accuracy in capturing the aerodynamics of both static and dynamic airfoil models, as discussed in Section 3.

A three-equation turbulence model of LKE K-K$_L$-ω was selected to evaluate the turbulence region. The description of the detailed equations and coefficients used in the model is referred to the references (Walters *et al.,* 2002 & Walters *et al.,* 2008). This turbulence model is capable of predicting the transition from laminar to turbulent flow in a simulation of flow around a body.

For the dynamic simulation, the stretching mesh technique was adopted to model the plunging airfoil (Validation study) and the oscillating trailing edge fringe simulations. This moving mesh technique enables the expanding and shrinking of the mesh elements depending upon the movement of the solid region, and thus avoids producing the pressure or velocity fluctuations at interfaces when using overset or discontinuous mesh, resulting from different grid sizes between the static and dynamic fields.

3. GRID SENSITIVITY STUDY AND THE DYNAMIC MOTION VALIDATION

The computational mesh sensitivity study was implemented using the bare airfoil S833 model by comparing the simulated drag and lift coefficients against experimental results (Somer *et al.,* 2005). The boundary conditions were defined based on the
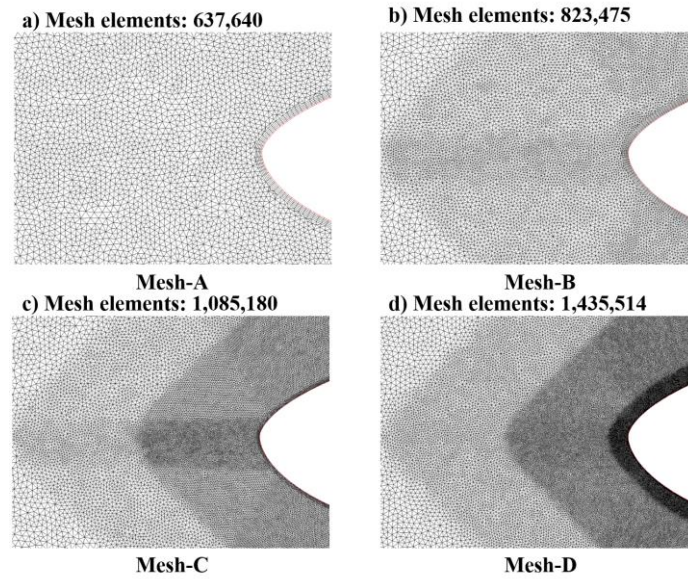
Fig. 2. Close-up views of four types of computational grids around the leading-edge of the airfoil. a) mesh-A with the mesh elements of 637,640; b) mesh-B with the mesh elements of 823,475; c) mesh-C with the mesh elements of 1,085,180; d) mesh-D with the mesh elements of 1,435,514.
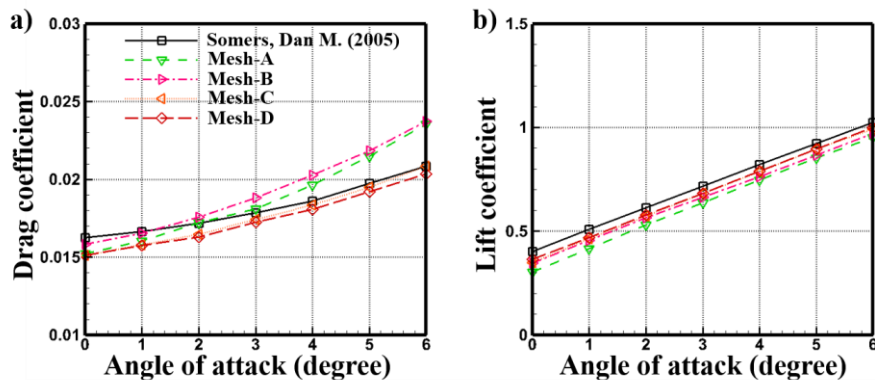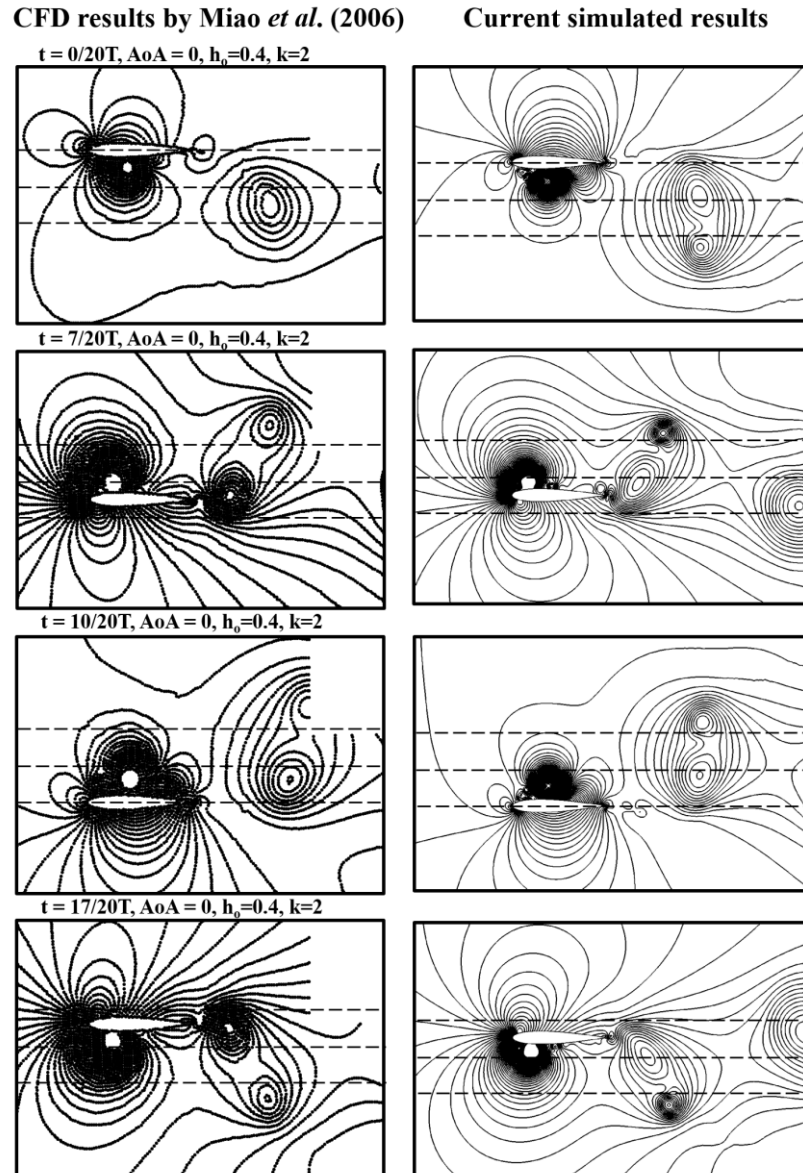

Fig. 3. a) Comparison of the drag coefficient with reference; b) the comparison of lift coefficient with reference.

R_e number of 4×10^5 in the experiment. Four different computational meshes were tested as shown in Fig. 2, and the resultant Y+ values were 1.43, 3.35, 10.13, and 19.92 for mesh-D to mesh-A, respectively. Seven AoAs of the airfoil were modeled, ranging from 0- to 6-degree. As can be seen in Fig. 3, mesh-C and mesh-D can provide accurate C_D and C_L coefficients compared to the experimental data with the overall difference being less than 10%. By considering the computational efforts, mesh-C was selected to carry out the simulations for the airfoil models equipped with a flapping trailing edge fringe.

The validation of the dynamic motion simulation was conducted to reproduce the pressure coefficient distribution around the airfoil with a plunging motion reported by Miao *et al.* (2006). The detailed description of the computational model and boundary conditions can be found in Miao *et al.* (2006). In brief, the airfoil NACA0014 was used as the computational model under the conditions of R_e

$= 4\times10^4$ and the plunging motion was defined as $h=ch_ocos(\omega t)$, where h is the instantaneous position of the airfoil; h_o is the dimensionless stroke amplitude; c is the chord length of the airfoil; ω is the angular oscillation frequency. Instead of using the dynamic moving mesh method defined by the user-defined-function utilized in the report, the current simulation employed a stretching moving mesh technique to model the plunging motion. The pressure coefficient distribution in the flow field at different timings was compared against the numerical results (Miao *et al.,* 2006).

Figure 4 shows the comparison of pressure coefficient distributions over the flow field when t = 0/20 T, 7/20 T, 10/20 T, and 17/20 T. As can be observed, the overall pressure contour can be captured very well by the current dynamic moving mesh technique. It might be noted that there are two vortices predicted behind the trailing edge at t = 0/20 T as compared to one vortex observed from the

CFD results by Miao *et al.* (2006)   Current simulated results

t = 0/20T, AoA = 0, h_o=0.4, k=2

t = 7/20T, AoA = 0, h_o=0.4, k=2

t = 10/20T, AoA = 0, h_o=0.4, k=2

t = 17/20T, AoA = 0, h_o=0.4, k=2

Fig. 4. Comparison of the pressure coefficient distributions of the laminar flow over rigid flapping airfoil model at t = 0/20 T, 7/20 T, 10/20 T, and 17/20 T between the current method (right side) and previous CFD results (left side) by Miao *et al.* (2006). The pressure coefficient ranges from -6.67 to 1.74.

report. However, from the pressure coefficient distribution at t = 17/20 T, two vortices were shed from the trailing edge before the airfoil reaches the top position. After 3/20 T the airfoil reaches the top position, these two vortices should be maintained and moved in a certain distance away from the trailing edge. Therefore, the two vortices obtained downstream when t = 0/20 T is more reasonable compared to the reference (Miao *et al.*, 2006). In sum, the selected mesh distribution mesh-C and moving mesh technique can be used to model the effect of the flapping fringe on the flow characteristics in the wake of the airfoil.

4. RESULTS AND DISCUSSION

The CFD simulation of flow over the airfoil S833

equipped with a flapping fringe was implemented. The bare airfoil model was defined as the baseline model for comparisons. The investigation primarily concentrated on the spanwise vorticity in the wake since it states the vortical velocity and turbulence of the fluid.

Figure 5 presents the simulated instantaneous and time-averaged vorticity distributions in the wake for the baseline model. The quasi-steady state was reached with evenly shed vortices. The frequency of the shedding vortices is f_s=140 Hz obtained through the calculation of PSD of the velocity in the wake. It results in a Strouhal number of St = 0.472, which is defined as St = $f_s c/U_\infty$, where U_∞ is the free stream velocity. The time-averaged vorticity distribution shows two straps of vortices with a similar magnitude but with negative and positive
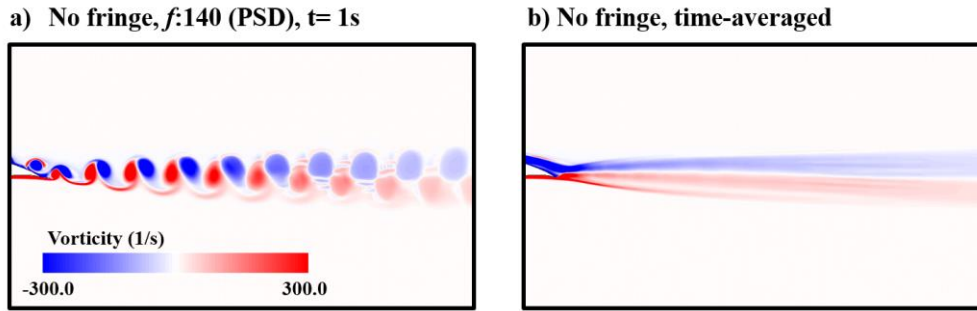
a) No fringe, *f*:140 (PSD), t= 1s

b) No fringe, time-averaged

Fig. 5. Vorticity distribution in the flow field. (a) represents the vorticity distribution at t = 1s. (b) represents the time-averaged vorticity distribution in the flow field.
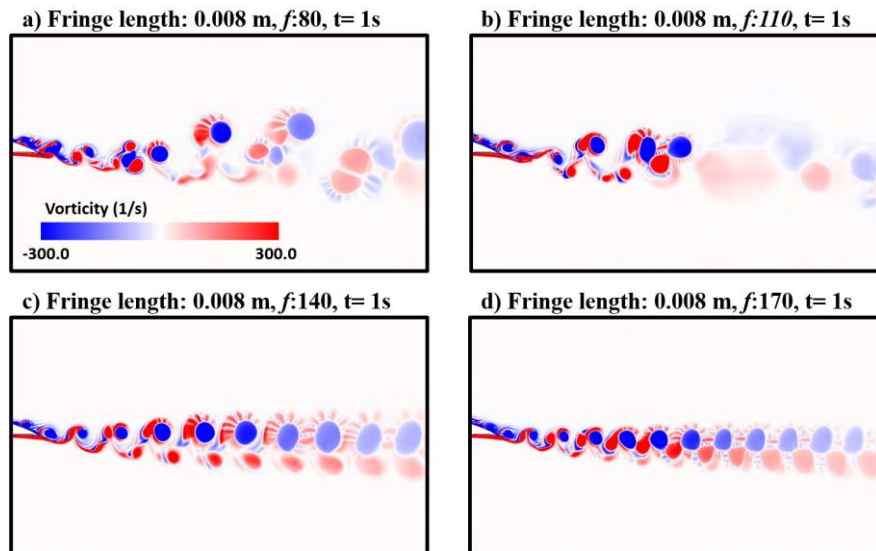
a) Fringe length: 0.008 m, *f*:80, t= 1s

b) Fringe length: 0.008 m, *f:110*, t= 1s

c) Fringe length: 0.008 m, *f*:140, t= 1s

d) Fringe length: 0.008 m, *f*:170, t= 1s

Fig. 6. Instantaneous vorticity distributions of the airfoil model with a fringe length of 0.008 m at t = 1s. (a) represents the airfoil model with $f = 80$ Hz. (b) represents the airfoil model with $f = 110$ Hz. (c) represents the airfoil model with the fringe flapping frequency of 140 Hz. (d) represents the airfoil model with $f = 170$ Hz.

values respectively and decaying along the flow direction. The Karman vortex street downstream of the airfoil, as shown in Fig. 5, is considered as a typical vortex shedding mechanism for the current R_e of 4×10^4. The following work will focus on the effect of flapping fringes on the vortex generation, interaction, shedding process, and decaying feature.

4.1 Instantaneous Vorticity Distributions for The Airfoil Equipped with Different Fringes

Figure 6 shows the instantaneous vorticity distributions for the airfoil model equipped with L_f = 0.008 m and coupled with various f. The airfoil model with $f = 140$ or 170 Hz shows evenly shed vortices compared to the baseline model, where the case with $f = 170$ Hz produces smaller gaps between each pair of vortices. In terms of the vortex structure, the airfoil model with $f = 140$ Hz tends to break the positive vortex into two parts distributed vertically with a similar magnitude. This behavior can also be observed from the model with $f = 170$ Hz. However, the positive vortices show relatively

weak strength surrounding the negative vortices, accelerating the dissipation. Nevertheless, when the fringe flapping frequency f is lower than f_s, the vortices are irregularly shed with a unique pattern and non-uniform scales and gaps between each pair. As can be observed, the airfoil model with $f = 80$ or 110 Hz can change the coherent structure of the large-scale shedding vortices, and at the same while, accelerate the vortex dissipation. This effect is particularly distinct for the model with = 110 Hz, which can be observed in Fig. 6(b).

Figures 7 and 8 present the instantaneous vorticity distributions at various flapping frequencies for the airfoil models with L_f = 0.01 and 0.012 m. Similar vortex shedding characteristics can be observed, where cases with low f (<140Hz) can change the coherent structure of the large-scale shedding vortices, accelerating the vortex dissipation. Overall, as the fringe length increases, the long fringe with $f = 170$ Hz breaks the negative vortex into two parts instead of breaking the positive ones compared to the vortices structure in Figs. 6 and 7. Changing the fringe length might not improve the
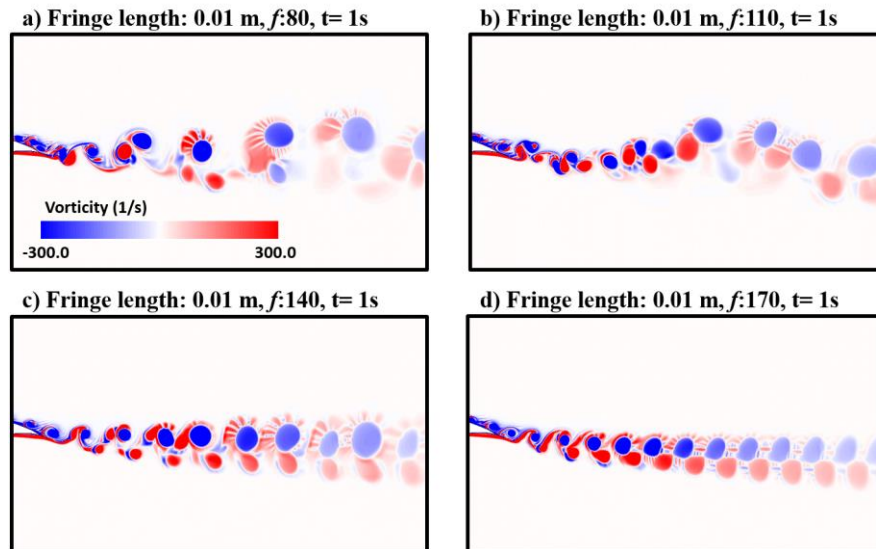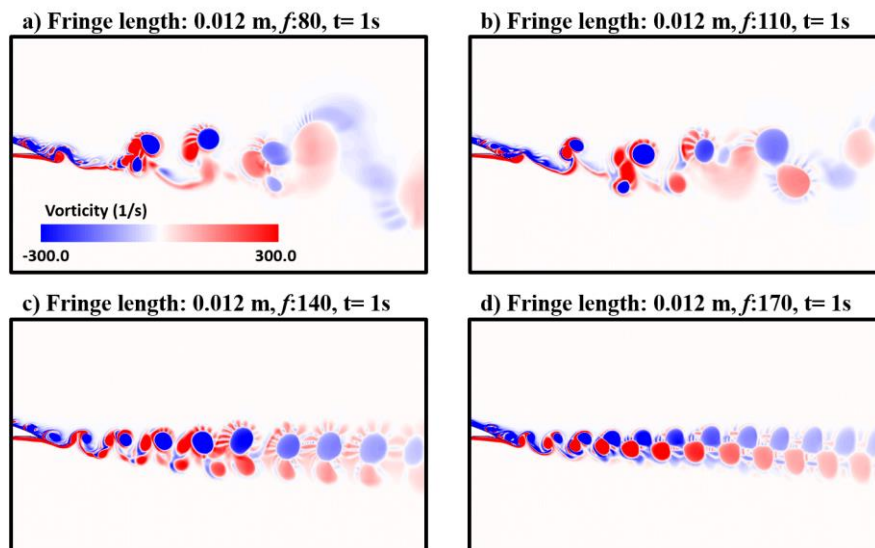
Fig. 7. Instantaneous vorticity distributions of the airfoil model with a fringe length of 0.01 m long at t = 1s. (a) represents the airfoil model with *f* = 80 Hz. (b) represents the airfoil model with *f* = 110 Hz. (c) represents the airfoil model with *f* = 140 Hz. (d) represents the airfoil model with *f* = 170 Hz.

Fig. 8. Instantaneous vorticity distributions of the airfoil model with a fringe length of 0.012 m long at t = 1s. (a) represents the airfoil model with *f* = 80 Hz. (b) represents the airfoil model with *f* = 110 Hz. (c) represents the airfoil model with *f* = 140 Hz. (d) represents the airfoil model *f* = 170 Hz.

structure of the shedding vortices as compared to the effects induced by varying the flapping frequency.

4.2 The Effect of the Fringe Motion on the Vortex Shedding

Figure 9 presents the power spectral densities of the velocity in the wake of the airfoils equipped with L_f = 0.01 and coupled with various f. The instantaneous velocity was sampled at 20000 Hz, and the total number of samples was 20000, leading to a frequency resolution of 1 Hz for the spectrum analysis. The PSD was performed using Welch's method with the default Hamming window

function, 50% overlay between segments, and the default FFT length. The results show that the vortex shedding frequencies are 80 Hz, 110 Hz. 140 Hz, and 170 Hz for each case, which is the same as the flapping frequency of the fringe accordingly. To observe the dissipation and coherent structure of a vortex accurately, attention was paid to one airfoil model (L_f =0.01 m) by tracing a negative vortex during one flapping cycle when it departs from the fringe end, as shown in Fig. 10. In-plane dashed lines crossing the same vortex and the values of the vorticity intensity at different timings were labeled to aid in understanding the propagation and decay of the shedding vortices. The original frequency of
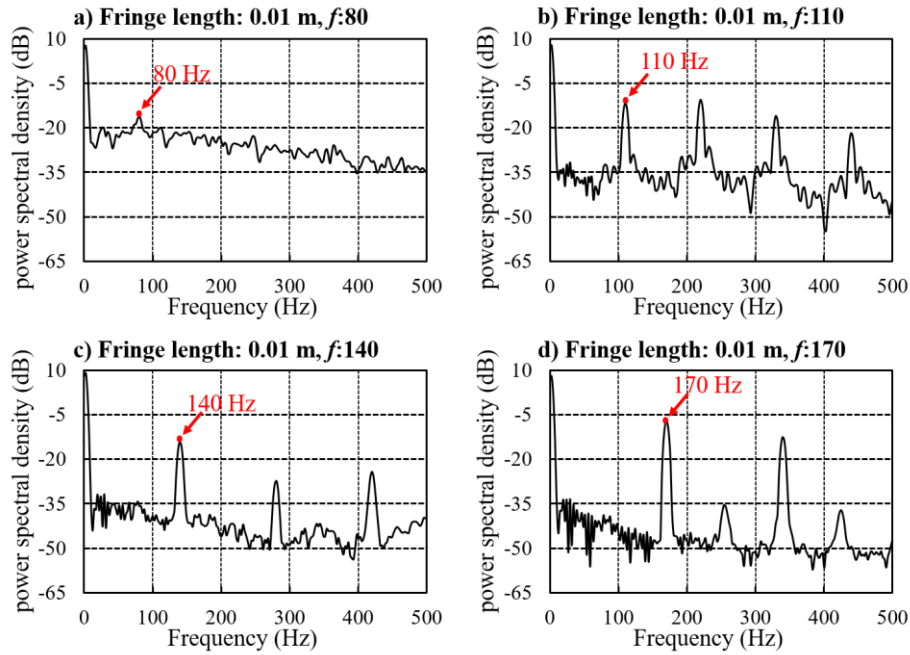
Fig. 9. Power spectral densities of the velocity in the wake of the airfoils equipped with a 0.008 m fringe.
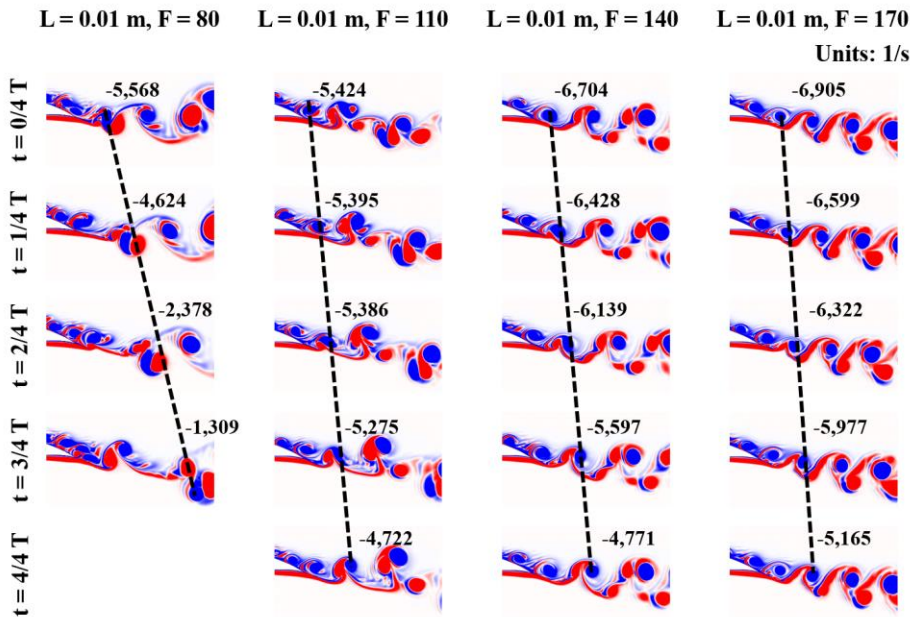

Fig. 10. The tracing of shedding vortices starts from the timing of the negative vortex departing from the fringe end. Values of the vorticity intensity at different timings are labeled at each time step.

vortex shedding from the bare airfoil (f_s = 140 Hz) is interfered by the intrusion of the vibrating fringe, which produces a pair of the vortex with opposite rotational direction. This offsetting effect varies at different flapping frequencies. The case with f = 80 Hz was merely plotted until 3/4 T since the negative vorticity intensity reaches a low offset value as that appeared at 4/4 T for other cases.

The vorticity magnitude at 0/4 T are similar between the models with f = 80 and 110 Hz, but

after 1/4 T, the magnitude is decreased by 16.95% and 0.53%, respectively. At 3/4 T, the vortex intensity is reduced by 76.5% for the case with f = 80 Hz and 2.75% for the case with f = 110 Hz. After one flapping cycle, only 12.9% of the initial vortex intensity is weakened for the case with f = 110 Hz. The vortex shedding patterns from the model with f = 80 and 110 Hz are truly irregular (as shown in Figs. 6, 7, and 8), indicating that these two cases shown in Fig. 10 are unrepresentative. On the other hand, the models with f = 140 and 170 Hz generate
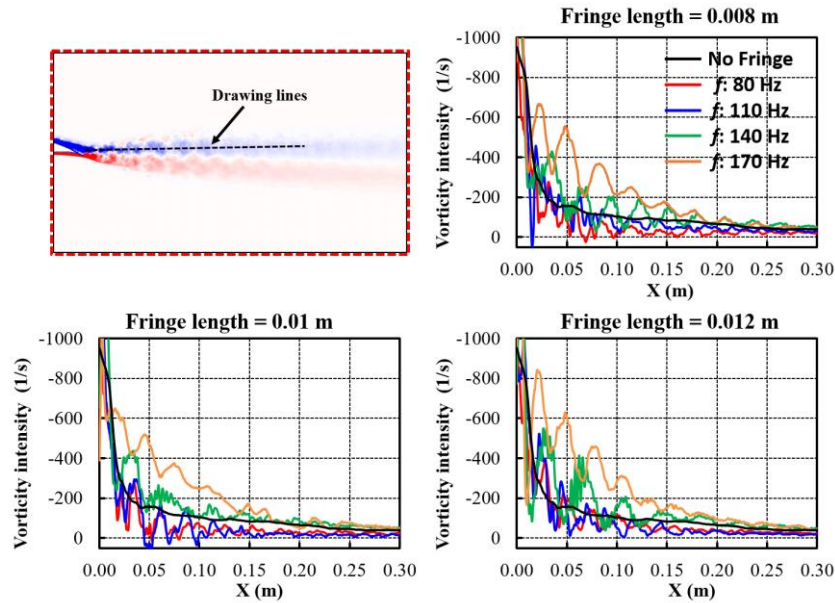
Fig. 11. Comparison of vorticity distribution along the dashed line through the vorticity region center of the anticlockwise vortices downstream of the trailing edge for the airfoil with and without the fringe.

similar Vertex intensity values of -6,704 and -6,905 1/s, respectively. After one flapping cycle, the vorticity intensity is reduced to -4,771 1/s (reduced by 28.8%) for the former case compared to -5,165 1/s (reduced by 25.2%) for the latter one. Overall, the flapping fringe can determine the vortex shedding frequency forcibly. As a result, the coherent structure and dissipation of the vortices in the wake are modified and attenuated dramatically. It is demonstrated that the flapping frequency of the fringe is the key factor to interfere the coherent vortex structure in the wake of the airfoil, where the low flapping frequency of the fringe (< 140 Hz) is able to produce relatively small-scale vortices and accelerate the dissipation of vortices, and as the flapping frequency increases, the flapping motion restrains from dissipating.

4.3 Time-averaged Vorticity Distributions

A track line along the center of the time-averaged negative vorticity region was created for each case, as shown in Fig. 11. The models with $f = 140$ and 170 Hz cannot provide improvements on the dissipation of the vorticity and even take opposite effects compared to the baseline model, as well as produce high oscillations of vorticity in the wake. On the other hand, the models with the $f = 80$ and 110 Hz show a similar vorticity magnitude along the track line. As for the fringe length, the model with $L_f = 0.01$ m provides a better improvement on the vorticity attenuation.

4.4 The Effect of the Flapping Fringe on C_D and C_L Coefficients

The trailing edge fringe not only reduces the vorticity in the wake of the airfoil but also decreases the drag coefficient and increases the lift

coefficient, as shown in Fig. 12. The drag and lift coefficients were calculated by integrating the pressure forces over the bare airfoil model in horizontal and vertical directions. Due to the fringe-induced oscillation of the forces, time-averaged pressure forces within the last 0.5s were used to compute the lift and drag coefficients. Since the goal of this work is to investigate the effects of the equipped flapping fringe on the bare airfoil, the drag and lift forces on the fringe were not considered. Regarding the lift coefficient of the fringe, the lift force acting on the fringe would additionally increase the overall lift of the airfoil, contributing an even larger lift coefficient.

Figure 12 demonstrates that the change in the C_D coefficient is opposite to the increase of the fringe length and flapping frequency, whereas the C_L coefficient is proportional to these two parameters. As a result, the model with $L_f = 0.012$ m and $f = 170$ Hz provides the minimum C_D of 19.5% lower and maximum C_L of 63.19% higher than that of the baseline model. However, this combination could not help in reducing the magnitude of shedding vortices in the wake of the airfoil. The C_D coefficients computed from the models with $f = 80$ Hz are similar to the baseline model, while the C_L coefficients can be enhanced. These findings are different from the effect of the serrated trailing edge, which tends to reduce the lift coefficient (Herr *et al.,* 2005). However, the lift enhancement is observed in a comprehensive study of an airfoil with a static extended trailing edge (Liu *et al.,* 2007). The changes in C_D and C_L coefficients are mainly attributed to the improved separation over the upper surface due to the flapping motion. The flapping fringe produces a long-strap region of lower negative pressure in the wake, which
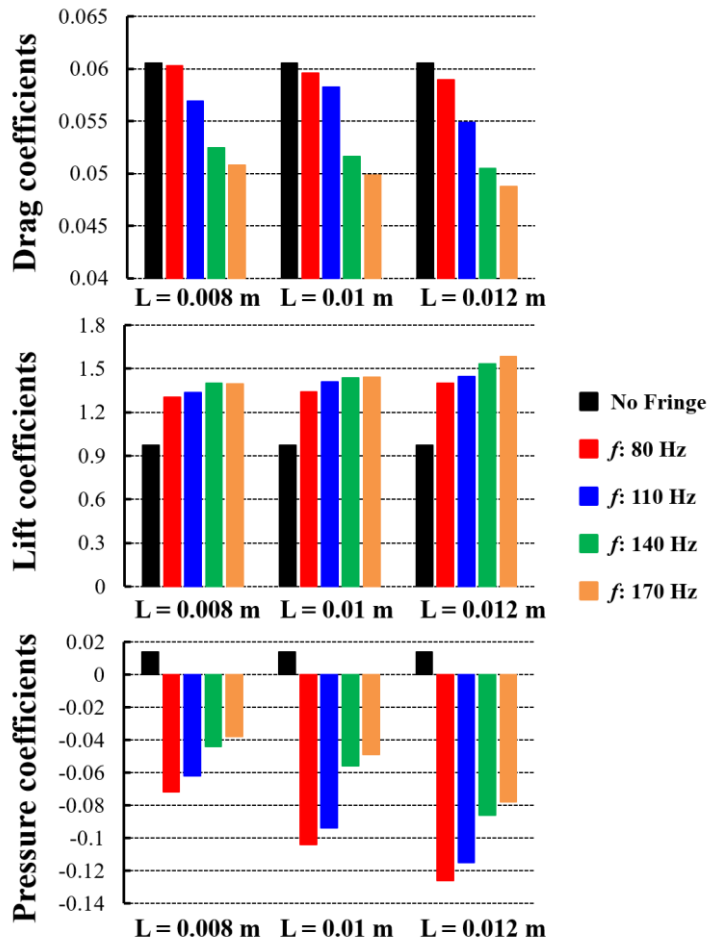
Fig. 12. Comparison of drag and lift coefficients for the airfoils equipped with various fringe lengths (m) and flapping frequencies (Hz) and the spatial-averaged pressure coefficient (C_p) in the wake of the airfoils, as the rectangular window shown in Fig. 13.
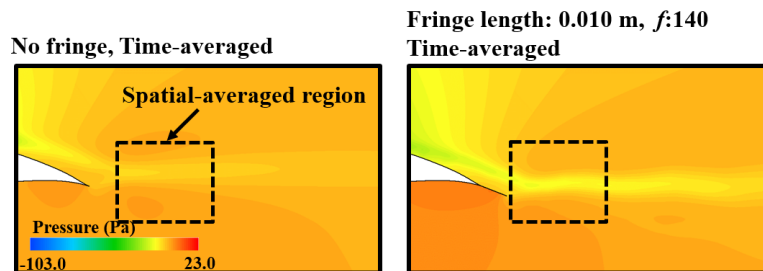

Fig. 13. Pressure distribution downstream of the airfoil without and with the fringe.

accelerates the upstream flow adjacent to this region through a "suction" effect and thus suppresses the separation over the airfoil. The suction effect has been illustrated in Fig. 13. The spatial- and temporal-averaged pressure coefficient was calculated over a selected rectangular window downstream of the trailing edge during the last one second. The pressure coefficient value for this average window in the downstream of the airfoil without fringe and with fringes were exhibited in Fig. 12. The current design of the fringe could generate a reduction of C_P by 0.06 ~ 0.14. It is

observed that the suction pressure magnitude increases with the increasing fringe length, in contrast, it decreases with the increasing flapping frequency. This low-pressure "suction" effect forces the flow to reattach on the upper surface of the airfoil, and thus finally results in an increased lift and decreased drag coefficient.

The effect of the flapping frequency f on the generation and dissipation of vortices in the wake has been investigated. It is found that a promotive f should be determined according to the f_s of the

baseline model. 1), if $f \geqslant f_s$, the vortices can be either maintained or enhanced by the vibration of the fringe. A higher f tends to serve as a booster to increase the local velocity at the trailing edge, resulting in the enhancement of the vorticity and reduction of the size of vortices. 2) if $f < f_s$, the frequency of the shedding vortices was slowed down, because of the disruption of the fringe on the original shedding pattern. As a result, the intensity of vortices became weak and easy to dissipate. Consequently, the f can be adjustable based on f_s of an airfoil model at different AoA, and the study of effects of the flapping frequency on the airfoil model with different AoA will be investigated in our future work. In the current work, the assumption of the mesh distribution and dynamic simulation of the vibrating motion may cause numerical errors. The validation study of the numerical approach for the flapping fringe airfoil model was not conducted due to the lack of comparable experimental data or numerical simulations results in the literature. However, the overall flow behavior is consistent with that observed in the experiment reported by Yang *et al.* (2015). Further experimental studies are demanded to verify the findings of the current investigation.

5. CONCLUSION

A 2D airfoil S833 equipped with a flapping fringe with AoA of 9-degree in a Reynolds number of 4×10^4 has been conducted to investigate the vortex shedding around the trailing edge. The effects of different fringe lengths and flapping frequencies on the vortex shedding and dissipation are studied. The simulation results of vorticity distributions in the wake demonstrate that the model with the fringe length of 10% of the chord length and flapping frequency $f = 110$ Hz could significantly reduce the strength of the shedding vortex, producing unique irregular vortices with smaller vorticity and fast decay rate. The flapping trailing edge fringe is able to alter the coherent structure of the large-scale trailing edge vortex, which could lead to accelerated vortex dissipation. The additional flapping trailing edge fringe can also achieve the reduction of the drag coefficient and enhancement of the lift coefficients through producing a suction region downstream of the fringe.

REFERENCES

Arndt, R. (1972). Effect of Leading-Edge Serrations on Noise Radiation from A Model Rotor. Society of Naval Architects and Marine Engineers, and U.S. Navy, *Advanced Marine Vehicles Meeting*, Annapolis, MD, USA

Chong, T. P., and P. F. Joseph (2013). An experimental study of airfoil instability tonal noise with trailing edge serrations. *Journal of Sound and Vibration* 332(24), 6335-6358.

Chong, T. P., P. F. Joseph and M. Gruber (2013). Airfoil Self Noise Reduction by Non-Flat Plate Type Trailing Edge Serrations. *Applied Acoustics* 74(4), 607-613.

Das, C.,A. Mimani, R. Y. Porteous and C. J. Doolan (2015). An experimental investigation of flow-induced noise mechanism of a flexible flat-plate trailing-edge. *Acoustics* 2015 Hunter Valley.

Finez, A., M. Jacob, E. Jondeau and M. Roger (2010). Broadband Noise Reduction with Trailing Edge Brushes. *16th AIAA/CEAS Aeroacoustics Conference,* Stockholm, Sweden.

Herr, M. and W. Dobrzynski (2005). Experimental Investigations in Low-Noise Trailing Edge Design. *AIAA Journal* 43(6), 1167-1175.

Hersh, A. S., P. T. Sodermant and R. E. Hayden (1974). Investigation of Acoustic Effects of Leading-Edge Serrations on Airfoils. *Journal of Aircraft* 11(4), 197-202.

Ito, S. (2009). Aerodynamic Influence of Leading-Edge Serrations on An Airfoil in A Low Reynolds Number. *Journal of Biomechanical Science and Engineering* 4(1), 117-123.

Jones, L. E. and R. D. Sandberg (2012). Acoustic and hydrodynamic analysis of the flow around an aerofoil with trailing-edge serrations. *Journal of Fluid Mechanics* 706, 295-322.

Kamps, L., C. Brücker, T. F. Geyer and E. Sarradj (2017). Airfoil self noise reduction at low Reynolds numbers using a passive flexible trailing edge. In *23rd AIAA/CEAS Aeroacoustics Conference* (p. 3496).

Kerho, M., S. Hutcherson, R. F. Blackwelder and R. H. Liebeck (1993). Vortex Generators Used to Control Laminar Separation Bubbles. *Journal of Aircraft* 30(3), 315-319.

Kim, J. W., S. Haeri and R. F. and Joseph (2016). On the reduction of aerofoil–turbulence interaction noise associated with wavy leading edges. *Journal of Fluid Mechanics* 792, 526-552.

Klän, S., M. Klaas and W. Schröder (2010). The Influence of Leading Edge Serrations On The Flow Field Of An Artificial Owl Wing. *28th AIAA Applied Aerodynamics Conference,* Chicago, Illinois.

Klän, S., T. Bachmann, M. Klaas, H. Wagner and W. Schröder (2009). Experimental Analysis of The Flow Field Over A Novel Owl Based Airfoil. *Experiments in Fluids* 46(5), 975-989.

Liang, G., J. Wang, Y. Chen, C. Zhou, J. Liang and L. Ren (2010). The Study of Owl's Silent Flight and Noise Reduction on Fan Vane with Bionic Structure. *Advances in Nature Science*

3(2), 192-198.

Lilley, G. (1998). A Study Of The Silent Flight Of The Owl. *4th AIAA/CEAS Aeroacoustics Conference,* Toulouse, France.

Liu, T., J. Montefort, W. Liou, S. R. Pantula and Q. A. Shams (2007). Static Extended Trailing Edge for Lift Enhancement: Experimental And Computational Studies. *3rd International Symposium on Integrating CFD and Experiments in Aerodynamics, U.S. Air Force Academy,* CO, USA.

Liu, X., H. Kamliya Jawahar, M. Azarpeyvand and R. Theunissen (2017). Aerodynamic Performance and Wake Development of Airfoils with Serrated Trailing-Edges. *AIAA Journal* 55(11), 3669-3680.

Miao, J. M. and M. H. Ho (2006). Effect of Flexure on Aerodynamic Propulsive Efficiency of Flapping Flexible Airfoil. *Journal of Fluids and Structures* 22(3), 401-419.

Moreau, D. J. and C. J. Doolan (2013). Noise-Reduction Mechanism of a Flat-Plate Serrated Trailing Edge. *AIAA Journal* 51(10), 2513-2522.

Narayanan, S., P. Chaitanya, S. Haeri, P. Joseph, J. W. Kim and C. Polacsek (2015). Airfoil noise reductions through leading edge serrations. *Physics of Fluids* 27(2), 025109.

Sarradj, E., C. Fritzsche and T. Geyer (2011). Silent Owl Flight: Bird Flyover Noise Measurements. *AIAA Journal* 49(4), 769-779.

Schlanderer, S. C. and R. D. Sandberg (2013). DNS of a Compliant Trailing-Edge Flow. In *19th AIAA/CEAS Aeroacoustics Conference* (p. 2013).

Shan, H., L. Jiang, C. Liu, M. Love and B. Maines (2008). Numerical Study of Passive And Active Flow Separation Control Over A Naca0012 Airfoil. *Computers & Fluids* 37(8), 975-992.

Soderman, P. T. (1973). Leading-Edge Serrations Which Reduce the Noise of Low-Speed Rotors. *NASA Technical Report,* TND-7371.

Somers, D. M. (2005). The S833, S834, and S835 Airfoils. *National Renewable Energy Laboratory*, Golden, CO, Report No. NREL/SR-500-36340.

Talboys, E. and C. Brücker (2018). Upstream shear-layer stabilisation via self-oscillating trailing edge flaplets. *Experiments in Fluids* 59(10), 145.

Talboys, E., T. F. Geyer and C. Brücker (2019). An aeroacoustic investigation into the effect of self-oscillating trailing edge flaplets. *Journal of Fluids and Structures*.

Veldhuis, L. L. M., D. P. Jansen, J. El Haddar and G. Correale (2012). Novel Passive And Active Flow Control For High Lift. *28th International Congress of the Aeronautical Sciences ICAS,* Brisbane, Australia.

Walters, D. K. and D. Cokljat (2008). A three-equation eddy-viscosity model for Reynolds-averaged Navier–Stokes simulations of transitional flow. *Journal of Fluids Engineering* 130(12), 121401.

Walters, D. K. and J. H. Leylek (2002). A new model for boundary-layer transition using a single-point RANS approach. *In ASME 2002 International Mechanical Engineering Congress and Exposition* 67-79.

Winzen, A., M. Klaas and W. Schroder (2014). PIV Measurements Comparing Natural and Model Owl Wings. *17th International Symposium on Applications of Laser Techniques to Fluid Mechanics*, Lisbon, Portugal.

Winzen, A., S. Klän, M. Klaas and W. Schröder (2012). Flow Field Analysis and Contour Detection Of A Natural Owl Wing Using PIV Measurements. *Nature-Inspired Fluid Mechanics, Springer,* Berlin, Heidelberg. ISBN-10: 3642283012.

Yang, Z., Z. He, H. Yu and F. Chen (2015). Study on the Vortex Wake of an Airfoil Equipped with Flexible Trailing Edge Fringe. *53rd AIAA Aerospace Sciences Meeting,* Kissimmee, Florida.